



ELSEVIER

Journal of Crystal Growth 198/199 (1999) 1032–1038

JOURNAL OF **CRYSTAL
GROWTH**

The effect of mismatch strain on Stranski–Krastanow transition in epitaxial $\text{Ge}_x\text{Si}_{1-x}/\text{Si}(001)$ gas-source growth

I. Goldfarb*, G.A.D. Briggs

Department of Materials, University of Oxford, Parks Road, Oxford OX1 3PH, UK

Abstract

Mechanisms of strain-relief during epitaxial growth of $\text{Ge}_{0.6}\text{Si}_{0.4}/\text{Si}(001)$ alloy at 500°C have been investigated using in situ scanning tunneling microscopy. The reduction of mismatch strain due to reduced Ge content of the epilayer (2.6% relative to 4.2% in $\text{Ge}/\text{Si}(001)$) has a profound effect not only on the final film morphology, but seem to alter the entire sequence of intermediate surface morphologies which, under these conditions, is dominated by layer-mounding rather than by faceting. Low-angle facets ($\approx 6^\circ$), different from the 11° - $\{501\}$ facets in the case of pure $\text{Ge}/\text{Si}(001)$, appear only at the final stages of growth. Understanding of roughening transitions in strained-layer growth is essential for controlling the cluster size and geometry for applications in quantum dot devices. © 1999 Elsevier Science B.V. All rights reserved.

PACS: 81.15.Kk; 61.16.Ch; 68.35.Bs; 68.65. + g

Keywords: Heteroepitaxy; Strain relaxation; Three-dimensional islands; Silicon; Germanium

1. Introduction

It has been recognised in the past decade that strained epilayers, e.g. $\text{Ge}_x\text{Si}_{1-x}/\text{Si}(001)$, where $0 < x < 1$, are metastable against surface roughening via three-dimensional (3D) faceted islands and ripples [1–8]. Since $\text{Ge}_x\text{Si}_{1-x}/\text{Si}$ is a Stranski–Krastanow (SK) growth system, the first few monolayers (ML) form pseudomorphic two-

dimensional (2D) wetting layer, prior to 3D roughening [9]. The kinetic route for strain relaxation exhibits a series of fascinating phenomena before reaching the final state of large 3D islands relaxed by dislocations: formation of two types of periodic vacancy lines [9–12] and the resultant reversal of the both surface stress anisotropy and step roughness [13,14], roughness dependence on the sign of the strain and triangular step instabilities [15–17], formation of various pyramidal micro- and macro-clusters with different facets [2,9,11,12], surface undulations [3,4,6–8] and, as we have recently demonstrated, the strain can also be partially relaxed via formation of pyramidal micro-pits [11].

* Corresponding author. Fax: +44 1865 273 783; e-mail: ilan.goldfarb@materials.ox.ac.uk.

In this letter we shed some light on this complex issue by real-time elevated-temperature scanning tunneling microscopy (STM) observation of $\text{Ge}_{0.6}\text{Si}_{0.4}/\text{Si}(001)$ growth from GeH_4 and Si_2H_6 . In order to increase the energy barrier for faceted islanding (which is extremely sensitive to strain [5]) the mismatch strain was reduced by introduction of Si into the growing film, however the ratio of partial GeH_4 and Si_2H_6 pressures was adjusted to 10 : 1 to ensure sufficient Ge presence ($x > 0.5$) for initial strain relief by roughening rather than by dislocations [5,6]. Such a reduction of strain in conjunction with relatively high growth temperature of 500°C was chosen to reduce the tendency for micro-hut formation [2]. As will be shown, such conditions lead to a sequence of surface structures different from those observed at lower temperatures and higher strains [11,12].

2. Experimental procedure

After ex vacuo chemical treatment the Si samples were introduced into a UHV JEOL JSTM-4500XT capable of operation up to 1250°C , degassed for several hours and repeatedly flashed at 1200°C (keeping the pressure below 10^{-7} Pa) before slow cooling to the desired temperature. Such treatment has generally proved effective in producing atomically flat good quality $\text{Si}(001)-(2 \times 1) \times (1 \times 2)$ surfaces free of mounds or pits [11,12,18]. The images were taken using electrochemically etched W tips at 500°C (achieved by direct current resistive heating and measured by optical pyrometer with $\pm 30^\circ\text{C}$ accuracy) in the “constant current” mode, with tunneling current of 0.08 nA and sample bias of -2 V while the 10 : 1 GeH_4 : Si_2H_6 mixture was fed through a precision-valve onto the sample mounted in the STM stage at a desired constant pressure in the 2×10^{-5} – 4×10^{-5} Pa range. The coverage was determined by computerised subtraction of submonolayer images from one another, after fixing the same fiducial points in each successive pair of images. The eventual thickness and the Ge content of the grown layer were measured using secondary ion mass spectroscopy (SIMS) depth profiling with a 7.5 keV, 5 nA O_2^+ primary beam. A reference sample with a 80 nm-thick

$\text{Ge}_{0.2}\text{Si}_{0.8}/\text{Si}(001)$ epilayer was used to calibrate the elemental sensitivity factors and the sputtering rate (which was also confirmed from the depth of the sputtered crater).

3. Results and discussion

SIMS depth profile of the grown $\text{Ge}_x\text{Si}_{1-x}$ epilayer is shown in Fig. 1 and exhibits three distinct regions: close to the surface, after the initial transient the profiles are relatively flat with a constant Si : Ge ratio (“epi”), followed by a region of gradually changing (“intermixed”) signals, which we attribute to sputter-induced atomic mixing and recoil implantation (e.g. see Ref. [19]), and, finally, below about 10 nm the profiles settle to values characteristic of the substrate, with some residual mixing of the Ge. Taking all these effects into account, especially sputtering of the Ge atoms over a depth of more than 10 nm, we estimate the Ge concentration of the epilayer to be 62%, which agrees with the composition to be expected from the 10 : 1 GeH_4 : Si_2H_6 mixture [20,21], and the epilayer thickness to be 2.5 nm, which agrees with 17 ML estimated from deposition rate (based on subtraction of successive images). Ge segregation to the surface was not detected in these SIMS profiles, although it could be masked by the initial transients.

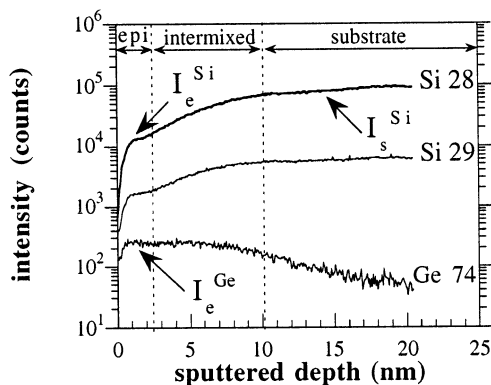


Fig. 1. SIMS depth profile of the grown $\text{GeSi}/\text{Si}(001)$ epilayer, with 7.5 keV, 5 nA O_2^+ primary beam (0.4 nm/min sputtering rate).

The evolution of surface morphology with coverage is shown in Fig. 2. The difference between the low surface coverage and higher coverages is striking: while initially the surface completely resembles that of a clean Si (Fig. 2a), with increasing coverage a high density of shallow pits is formed (Fig. 2b), followed by periodic array of dimer-vacancy-lines (DVLs) (Fig. 2c), and finally large faceted clusters (Fig. 2d). While in the case of pure Ge/Si(0 0 1) DVLs and dimer row vacancies (DRVs) were first to form [12], in the alloy case the pits preceded DVLs, and DRVs (forming the $(M \times N)$ -reconstructed surface when combined with DVLs [11]) did not form at all. Nucleation of the shallow pits proceeds similarly to that of hut pits observed in our previous work [11]: comparing the pair of surface voids in Fig. 2a to the same pair in Fig. 2b and Fig. 2c, it can be deduced that the shallow pits nucleate heterogeneously from the small existing voids. However these shallow pits (Fig. 3a) differ from the Ge/Si(0 0 1) hut pits described in our previous work [11] (Fig. 3b): their edges are oriented in the $\langle 1\ 1\ 0 \rangle$ crystallographic directions, and the wetting layer at the time of their formation is not sufficiently thick to accommodate an inverse pyramid, and thus the pits are too shallow to form a facet. Therefore they can mostly expand laterally, without gaining too much depth. Such a growth mode is realised by agglomeration of vacancies around the pits (there seems to be an apparent reluctance to fill them), as follows from examination of pit blow-ups in Fig. 3a and in the insets of Fig. 2a, Fig. 2b, and Fig. 2c.

In spite of this initial reluctance, as the growth continues the shallow pits are gradually filled and the strain can no longer be relieved at them, nor it can be relieved by DVLs since the mutual repulsion prevents them from further multiplication [10]. This point occurs at the coverage of 9 ML and indicates the beginning of SK transition. Fig. 4 shows an initially 2D island, which with increasing coverage (Fig. 4a and Fig. 4b) progressively evolves into the rather large and faceted 3D island (marked “2” in Fig. 2d), as seen in Fig. 4c and Fig. 4d. Fig. 5a displays profile plots measured along the lines indicated in Fig. 4, and Fig. 5b, demonstrates the island inclination angle dependence on coverage. Analysing the changes in cluster

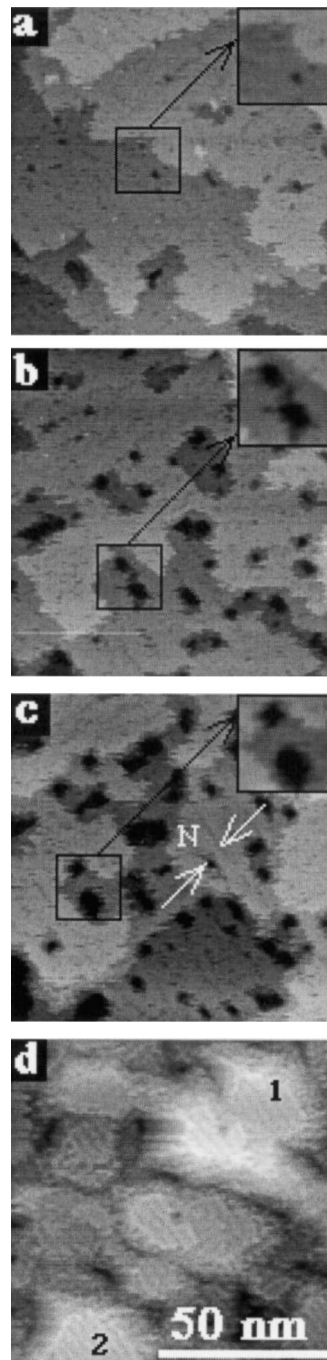


Fig. 2. Progression of $\text{Ge}_{0.6}\text{Si}_{0.4}/\text{Si}(0\ 0\ 1)$ growth at 500°C : (a) 0.3 ML; (b) 1.8 ML, conversion of voids into shallow pits (c) 3.0 ML: pit growth and formation of $(2 \times N)$; (d) 12 ML, formation of faceted clusters.

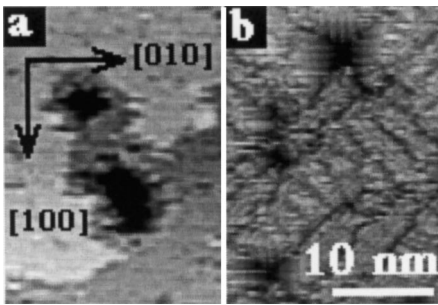


Fig. 3. Comparison of the shallow pits formed in this study (a) with the Ge/Si(0 0 1) hut pits from our previous work (b).

shape with coverage in Figs. 4 and 5a yields initial mounding of 2D layers on the island (Fig. 4a and Fig. 4b) with subsequent formation of low angle facet when a certain height is reached (Fig. 4c and Fig. 4d). Thus unlike the abrupt formation of faceted 3D clusters/pits in the pure Ge/Si(0 0 1) case [11,12], this transition takes place gradually over an interval of three monolayers: before the facet is formed the slope of the island wall gradually decreases from about 11° at 9 ML to about 6° for a facet formed at 12 ML, and then remains remarkably constant (see Fig. 5b). The resulting faceted island shapes are far less perfect and their sizes are 2–3 times larger when compared to a small typical Ge/Si(0 0 1) microhut of an ideal pyramidal shape (such a microhut from our previous work [11,12,18] is given for comparison in Fig. 4e). Larger cluster sizes are expected at lower strains and higher temperatures, as the terminal cluster width is inversely proportional to the square of strain [22], and higher growth temperatures promote lower nucleation rates [5] and larger terminal cluster widths.

In order to separate the effects of strain and temperature on the evolution of surface morphology, we have grown pure Ge/Si(0 0 1) under identical temperature and flux conditions. The evolution of surface morphology for this case is shown in Fig. 6, and it is not principally different from the Ge/Si(0 0 1) surfaces grown at lower temperatures [11,12], i.e. the initial Si(0 0 1)-like (2×1) reconstruction changes with coverage into $(2 \times N)$ (Fig. 6a and Fig. 6b), then into $(M \times N)$ and hut pits (Fig. 6c), and, eventually, into hut clusters

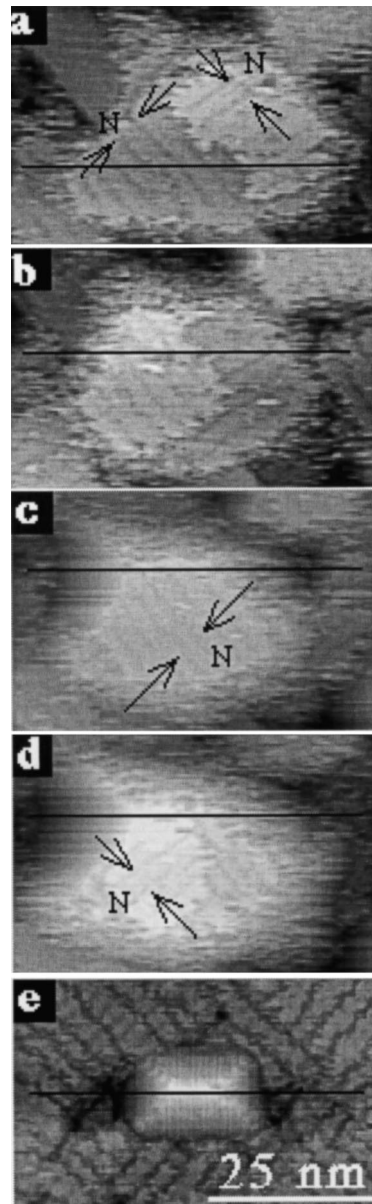


Fig. 4. Constant-current STM images of evolution of the island surface profile with coverage: (a) 9 ML, (b) 9.8 ML, (c) 12 ML and (d) 13 ML; (e) a typical Ge/Si(0 0 1) hut cluster from our previous work is included for comparison.

(Fig. 6d). The sizes of these huts are indeed comparable with the $\text{Ge}_{0.6}\text{Si}_{0.4}/\text{Si}(0 0 1)$ islands (i.e. compare the two huts in Fig. 6d to the islands “1” and “2” in Fig. 2d), however their shapes are still

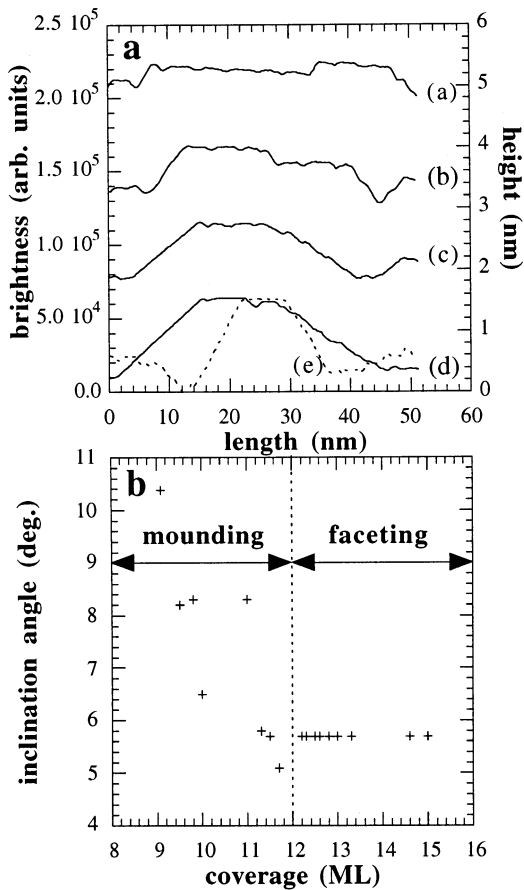


Fig. 5. (a) Surface profile plots taken along the black lines indicated in Fig. 4. Small (a)–(e) lettering corresponds to the (a)–(e) frames in Fig. 4. Note the change of the growth mode from stepped one (profiles (a) and (b)) to faceted (profiles (c) and (d)), as well as the difference between the facet slope of the large clusters in this study (profiles (c) and (d)) and the microhut (profile (e)). (b) Variation of the island wall inclination angle with coverage. Note the continuous slope decrease followed by the sharp transition to faceted mode at 12 ML and further constant slope value.

geometrically perfect, with rectangular $\langle 100 \rangle$ -oriented bases and $\{501\}$ facets. It thus could be concluded that the different evolution of the $\text{Ge}_{0.6}\text{Si}_{0.4}/\text{Si}(001)$ surface was caused solely by the reduction of misfit strain.

These observations partly corroborate the previous annealing experiments of Chen and co-workers of a 2 nm-thick $\text{Ge}_{0.5}\text{Si}_{0.5}$ layer at 590°C [23]. However, while their RHEED measurements

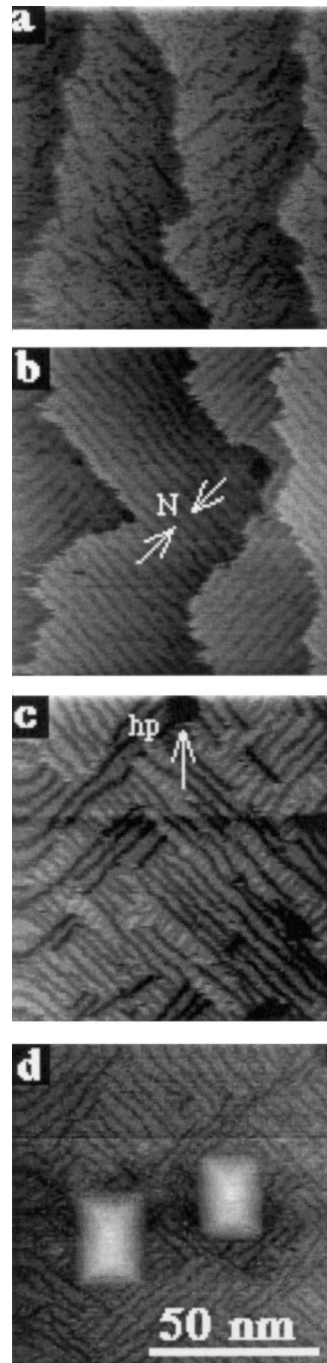


Fig. 6. Progression of $\text{Ge}/\text{Si}(001)$ growth at 500°C: (a) 0.5 ML, (b) 1.8 ML, perfect $(2 \times N)$ reconstruction, (c) 6.0 ML, formation of $(M \times N)$ and hut pits (hp), (d) 9.5 ML, formation of hut clusters.

indicated eventually $\{501\}$ faceting, the 6° inclination angle from our slope measurements were more consistent with $\{811\}$, $\{801\}$, $\{911\}$ or $\{901\}$ facets, which can also be regarded as vicinal (001) surfaces. Chen and co-workers have also observed continuous distribution of the mean facet inclination angle up to 11.3° [24]. Hence they have concluded that the energy barrier for the 2D–3D SK-transition occurs prior to the formation of discrete $\{501\}$ facets, and the kinetic pathway is dominated by the interaction between the steps comprising the facet rather than by the geometrical form of the facet surface energy. For this to happen, the energy barrier for the non-faceted nucleation must be smaller than that for the faceted one [24].

Evidence of $\{811\}$ facets in RHEED patterns from $\text{Ge}_{0.6}\text{Si}_{0.4}$ alloy has been reported [20], which is consistent with our STM slope measurements. However the exact structure of such a facet seems to be more complex than a simple description of a vicinal plane making a $6\text{--}7^\circ$ angle with (001) surface and which therefore consists of monoatomic steps separated by ≈ 1.1 nm wide terraces. In Fig. 4c and Fig. 4d the 3D island facets are $(2 \times N)$ reconstructed, just as the 2D islands and interisland layer (Fig. 2d, Fig. 4a and Fig. 4b). To our best knowledge such shallow facets have never been imaged before, and certainly this is the first observation of DVLs on island facets. Applying vicinal analog for such a facet one would expect 90° rotation of DVLs on each successive terrace of the facet, producing zig-zag pattern larger in magnitude but similar to the one formed by rotation of dimer rows on $\{501\}$ facets [2]. Fig. 4 proves this not to be the case; DVL orientation over the entire facet surface does not change until the next layer begins to grow on that facet (see Fig. 4d), in the precisely same fashion as on the previously 2D island (see Fig. 4a and Fig. 4b).

4. Summary

We have analysed the effects of growth parameters, such as the misfit strain and substrate temperature, on the Stranski–Krastanow roughening

transition in heteroepitaxial Ge-rich $\text{Ge}_x\text{Si}_{1-x}/\text{Si}(001)$ growth from gas sources. The interplay between various strain-relieving mechanisms can be treated in the framework of kinetic rates for corresponding processes as a function of these parameters, as has been derived by Tersoff and LeGoues [5]. Such an approach accounts well for the faceted appearance of even the critical cluster and pit nuclei in our previous work [11]. Under different sets of growth conditions other processes can dominate surface phenomena in pseudomorphic growth, e.g. nucleation of misfit dislocations [5] or stress-driven step-bunching [25]. When growing $\text{Ge}_{0.6}\text{Si}_{0.4}/\text{Si}(001)$ alloy the particular combination of higher temperature and lower mismatch strain (2.6% instead of 4.2% in $\text{Ge}/\text{Si}(001)$) had an effect of destabilisation of microhuts on one hand, and lowering the step formation free energy on the other hand, facilitating profusion of vacancy mounding around pits and later layer mounding on 2D islands (Fig. 2a and Fig. 2c, Fig. 4a and Fig. 4b, respectively). This type of kinetic approach proves effective in determining the initial stages, however when a mound reaches a certain size an ordered facet is energetically favourable to stepped island surface which also facilitates a more effective relaxation by dilatation of vertical lattice planes at the apex of a pyramid. The transformation of a stepped island into a faceted one is achieved by gradually lowering the inclination angle of the island wall down to about 6° , at which point the facet is nucleated. Once formed the facets remain stable and further growth proceeds by material addition to them.

The ability to control sizes, shapes and crystal-line perfection of the three-dimensional islands resulting from strained Stranski–Krastanow growth, is paramount for their applications in self-assembled quantum dot devices.

Acknowledgements

The authors wish to thank M. Eizenberg for providing the reference samples for SIMS calibration. This work is supported by EPSRC (GR/K08161).

References

- [1] D.J. Eaglesham, M. Cerullo, *Phys. Rev. Lett.* 64 (1990) 1943.
- [2] Y.-W. Mo, D.E. Savage, B.S. Swartzentruber, M.G. Lagally, *Phys. Rev. Lett.* 65 (1990) 1020.
- [3] A.J. Pidduck, D.J. Robbins, A.G. Cullis, W.Y. Leong, A.M. Pitt, *Thin Solid Films* 222 (1992) 78.
- [4] A.G. Cullis, D.J. Robbins, A.J. Pidduck, P.W. Smith, *J. Crystal Growth* 123 (1992) 333.
- [5] J. Tersoff, F.K. LeGoues, *Phys. Rev. Lett.* 72 (1994) 3570.
- [6] A.G. Cullis, *MRS Bull.* 21 (4) (1996) 21.
- [7] D.E. Jesson, K.M. Chen, S.J. Pennycook, *MRS Bull.* 21 (4) (1996) 31.
- [8] D.E. Jesson, K.M. Chen, S.J. Pennycook, T. Thundat, R.J. Warmack, *Phys. Rev. Lett.* 77 (1996) 1330.
- [9] M. Tomitori, K. Watanabe, M. Kobayashi, O. Nishikawa, *Appl. Surf. Sci.* 76/77 (1994) 323.
- [10] X. Chen, F. Wu, Z. Zhang, M.G. Lagally, *Phys. Rev. Lett.* 73 (1994) 850.
- [11] I. Goldfarb, P.T. Hayden, J.H.G. Owen, G.A.D. Briggs, *Phys. Rev. Lett.* 78 (1997) 3959.
- [12] I. Goldfarb, J.H.G. Owen, P.T. Hayden, D.R. Bowler, K. Miki, G.A.D. Briggs, *Surf. Sci.* 394 (1997) 105.
- [13] F. Wu, X. Chen, Z. Zhang, M.G. Lagally, *Phys. Rev. Lett.* 74 (1995) 574.
- [14] F. Wu, M.G. Lagally, *Phys. Rev. Lett.* 75 (1995) 2534.
- [15] Y.H. Xie, G.H. Gilmer, C. Roland, P.J. Silverman, S.K. Buratto, Y.J. Cheng, E.A. Fitzgerald, A.R. Kortan, S. Schupler, M.A. Marcus, P.H. Citrin, *Phys. Rev. Lett.* 73 (1994) 3006.
- [16] D.E. Jones, J.P. Peltz, Y.H. Xie, P.J. Silverman, G.H. Gilmer, *Phys. Rev. Lett.* 75 (1995) 1570.
- [17] K.M. Chen, D.E. Jesson, S.J. Pennycook, M. Mostoller, T. Kaplan, T. Thundat, R.J. Warmack, *Phys. Rev. Lett.* 75 (1995) 1582.
- [18] I. Goldfarb, P.T. Hayden, J.H.G. Owen, G.A.D. Briggs, *Phys. Rev. B* 56 (1997) 10459.
- [19] J.C. Vickerman, A. Brown, N.M. Reed (Eds.), *Secondary Ion Mass Spectrometry: Principles and Applications*, Clarendon Press, Oxford, 1989.
- [20] Y. Koide, A. Furukawa, S. Zaima, Y. Yasuda, *J. Crystal Growth* 115 (1991) 365.
- [21] Z. Zhang, private communication.
- [22] W. Dorsch, H.P. Strunk, H. Wawra, G. Wagner, J. Groenen, R. Carles, *Appl. Phys. Lett.* 72 (1998) 179.
- [23] K.M. Chen, D.E. Jesson, S.J. Pennycook, T. Thundat, R.J. Warmack, *J. Vac. Sci. Technol. B* 14 (3) (1996) 2199.
- [24] K.M. Chen, D.E. Jesson, S.J. Pennycook, T. Thundat, R.J. Warmack, *Phys. Rev. B* 56 (1997) R1700.
- [25] J. Tersoff, Y.H. Phang, Z. Zhang, M.G. Lagally, *Phys. Rev. Lett.* 75 (1995) 2730.